Journal of Applied Geophysics 123 (2015) 188–193

Contents lists available at ScienceDirect

Journal of Applied Geophysics

journal homepage: www.elsevier.com/locate/jappgeo

Pumping test in a layered aquifer: Numerical analysis of self-potential signals

Konstantin Titov [a,*], Pavel Konosavsky [a], Mikhail Narbut [b]

[a] St. Petersburg State University, Institute of Earth Sciences, 7-9 Universitetskaya naberezhnaya, 199034 St. Petersburg, Russia
[b] St. Petersburg State University, Faculty of Mathematics and Mechanics, 28 Universitetskii prospect, Staryi Petergof, 198504 St. Petersburg, Russia

ARTICLE INFO

Article history:
Received 20 May 2015
Received in revised form 9 October 2015
Accepted 12 October 2015
Available online 22 October 2015

Keywords:
Pumping test;
Numerical modeling;
Self-potential

ABSTRACT

We used numerical modeling to study self-potential (SP) signals associated with a pumping test in a layered aquifer containing the main aquifer, a thin aquitard, and a shallow aquifer. The results revealed an unusual behavior of SP signals, which were not linearly correlated with the hydraulic head distributions. We explained this behavior by a vertical downward groundwater flow, from the shallow aquifer to the main aquifer, in the course of the pumping test. However, when plotted as a function of time, the SP signals and hydraulic heads displayed coherent behavior. In both distributions, three stages of the pumping test were determined: at early times, only the main aquifer and the aquitard responded to the pumping; at intermediate times, the downward flow from the shallow aquifer occurred; and at late times, the layered aquifer responded to the pumping as a whole. The SP signals reacted to the sequence of these stages much faster than the hydraulic head distributions. In principle, this might allow reducing the duration of the pumping tests without losing valuable information.

1. Introduction

In the last decades, there has been an increased interest in application of self-potential (SP) method to investigation of groundwater flow, especially in cases of pumping and infiltration tests (e.g., Vasconcelos et al., 2014; Jardani et al., 2009; Bolève et al., 2007; Titov et al., 2005; Rizzo et al., 2004).

Some pioneering works in this area have been done by the Russian researchers (e.g., Murashko et al., 1981; Semenov, 1981; Bogoslovsky and Ogilvy, 1973; Gorelik and Nesterenko, 1956), who have shown measurable SP signals in response to pumping tests. Later on Suski et al. (2006), Titov et al. (2005), Rizzo et al. (2004) used quasi-linear relationships between the hydraulic head data and SP signals, which allowed considering SP signals as a proxy of piezometric level.

In recent works, a general approach has been developed to perform hydraulic conductivity tomography using the joint inversion of SP signals and groundwater head data. The hydraulic conductivity distribution within a synthetic heterogeneous aquifer was defined through the use of adjoint-state method (Ozaki et al., 2014; Soueid Ahmed et al., 2014). In a very recent paper, Chidichimo et al. (2015) assessed the saturated hydraulic conductivity in a conditions of large (field comparable scale) laboratory setup using a coupled model based on the modified Richards equation coupled with the Poisson equation providing the SP signals. The inversion was performed on the basis of the Spars Nonlinear Optimizer (Gill et al., 2005).

Although this very general approach had been addressed in previous works, experimental or numerical relationships between the hydraulic head data and SP signals are still of interest because they determine sensitivity of SP signals to the hydraulic head variation. As mentioned above, these relationships are frequently considered quasi-linear, which was confirmed by experimental and numerical data (see also Jardani et al., 2009). The linear relationship results in an SP signal distribution whose shape represents a “mirror image” of the water table (e.g., Darnet et al., 2003). Also, in steady state conditions, the electrical potential decreases as the inverse of the distance from the pumping well (Straface et al., 2011; Rizzo et al., 2004). The above-mentioned features of SP signals are typical of pumping tests in isolated aquifers. Two semi-analytical solutions for SP signals associated with pumping tests in isolated aquifers have been developed: the SP responses to pumping tests in confined (Malama et al., 2009a) and unconfined (Malama et al., 2009b) aquifers. These models also confirm a quasi-linear relationship between the drawdowns and the SP signals.

Vasconcelos et al. (2014) studied SP signals produced by pairs of injecting and pumping wells in an isolated aquifer using a tank experiment and numerical modeling. They compared electrical potentials for the cases of (1) SP produced by pumping and injection and (2) electrical potential produced by electrical sources (positive and negative) located at the same points that had been used for pumping. They showed that, in homogenous medium, these potentials have the same bipolar

* Corresponding author.
E-mail addresses: k.titov@spbu.ru (K. Titov), p.konosavskii@spbu.ru (P. Konosavsky), narbut2010@yandex.ru (M. Narbut).

http://dx.doi.org/10.1016/j.jappgeo.2015.10.006
0926-9851/

pattern. In contrast, in the presence of inhomogeneities, the SP and the electrical potential produced by electrical sources are different, which could be used as a field criterion for detecting inhomogeneities near pumping/injections wells.

Therefore to date, to the best of our knowledge, SP signals associated with pumping tests in layered aquifers have not been studied. An exception is a recent paper (Malama, 2014) where a new semi-analytical solution was derived (and validated by a sandbox experiment) for SP signals produced by pumping tests in unconfined aquifer including an impact of the vadose zone.

In this paper, we present a numerical study of SP signals produced by a pumping test in a layered aquifer that includes the main aquifer, a thin intermediate aquitard, and a shallow aquifer. We analyze the sensitivity of SP signals to hydraulic head variation, and we compare our results with those obtained by Malama (2014).

1.1. Physical background

For completely saturated sediments, the total electrical current density is composed of two components:

$$j = -\sigma\nabla\phi - L\nabla h, \tag{1}$$

where σ (in S m^{-1}) and L (in Am^{-2}) are the electrical conductivity and electrokinetic current coupling coefficient, respectively, φ (in V) and h (in m) are the electrical potential and the hydraulic head, respectively. The first term in the right-hand part of Eq. (1) is the Ohmic current density, and the second term is the streaming current density, produced by a drag of charged water within pore space (e.g., Ishido and Mizutani, 1981).

In the quasi-static limit, and according to the charge conservation, the total current density is divergence-free,

$$\nabla \cdot j = 0. \tag{2}$$

Substituting Eq. (1) into Eq. (2) leads to the Poisson equation for the electrical potential in heterogeneous porous medium (e.g., Sill, 1983):

$$\nabla(\sigma\nabla\phi) = -\nabla(L\nabla h) = J, \tag{3}$$

where J in Am^{-3} represent the source term.

The hydraulic head is described by the diffusion equation,

$$\nabla \cdot (K\nabla h) = S\frac{\partial h}{\partial t} + q, \tag{4}$$

where K is the hydraulic conductivity (in m s^{-1}), S is the storage coefficient (in m^{-1}), and q is the pumping rate (in s^{-1}). By solving Eq. (4) for the hydraulic head, one obtains the hydraulic head distribution, the source term in Eq. (3), and the electrical potential for the given electrical conductivity distribution.

A new formulation of the streaming potential problem (e.g., Bolève et al., 2007; Revil and Leroy, 2004) provides a link between the aforementioned coefficient and the hydraulic conductivity. According to the new formulation, a new parameter, Q_V is defined as an effective charge density (of the diffusion layer) per unit pore volume that is dragged by the flow of the pore water (Revil and Mahardika, 2013). The streaming current density is a product of Q_V and the Darcy velocity, **u**:

$$-L\nabla h = Q_v\mathbf{u}. \tag{5}$$

Based on experimental data, Bolève et al. (2009) showed a link between Q_V and the permeability, k, and Soueid Ahmed et al. (2014) converted this link for the hydraulic conductivity, K

$$\log(Q_V) = -3.49 - 0.82\log_{10}(K). \tag{6}$$

Combining Eqs. (5) and (6), a relationship between the electrokinetic current coupling coefficient and the hydraulic conductivity is obtained:

$$L = \hat{Q}_V K = 3.24 \cdot 10^{-4} K^{0.18}, \tag{7}$$

where K is expressed in m s^{-1}.

In the modeling, we used Eq. (7) to define values of the electrokinetic current coupling coefficient.

1.2. Description of models and definition of model parameters

We analyzed a model containing two aquifers separated by an aquitard. In the model, we used hydraulic properties typical of sandy aquifer and clayey aquitard (e.g., Bear, 1979). Based on the assumed values of the hydraulic conductivity and Eq. (7), we assessed the electrokinetic coupling coefficient values. Assuming that the aquifer contained fresh water, we set its electrical conductivity value at 10^{-2} S m^{-1}. Assuming that the clayey aquitard was characterized by a surface conductivity, we set its electrical conductivity twice higher than that of the aquifer ($2 \cdot 10^{-2}$ S m^{-1}). The single confined aquifer model (where the aquifer coincides with the main aquifer of the layered model) served as the reference model. The model parameters are summarized in Table 1.

1.3. Modeling method

We modeled SP signals on the basis of a conventional three-step method (Sill, 1983). First, Eq. (4) was solved with appropriate (Neumann or Dirichlet) boundary conditions for the hydraulic head. Then, electrical sources were calculated on the basis of the previously obtained hydraulic head distribution. Finally, the electrical potential was calculated by solving Eq. (3) with the appropriate boundary conditions for the electrical potential. The procedure of solving the differential equations was based on the finite-difference method with strictly implicit scheme (e.g., Press et al. 1992, p. 839; McDonald & Harbaugh 1988) and on the basis of the Libman method (Grunevald, 1971). The modeled area was broken up into rectangular cells of different sizes. The length of the cells increased with the distance from the pumping well, r, in geometric progression, and the width of the cells, a, increased so that $a = 2\pi r$. This produced a cylindrical coordinate system appropriate for modeling pumping wells. The finite difference discretization of Eqs. (3) and (4) produced two systems of linear equations, which were solved using the Gauss–Seidel iteration procedure with overrelaxation

Table 1
Model parameters.

Model	Pumping rate, L s^{-1}	Aquifer parameters					Aquitard parameters					Overlapping layer parameters	
		K, m s^{-1}	S_s, m^{-1}	S_y, –	σ, S·m^{-1}	L, 10^5 A m^2	K, m s^{-1}	S_s, m^{-1}	S_y, –	σ, S·m^{-1}	L, 10^5 A m^2	σ, S·m^{-1}	L, 10^5 A m^2
Single aquifer	0.463	$1.16\cdot10^{-5}$	10^{-4}	0.09	10^{-2}	4.18	–	–	–	–	–	10^{-2}	4.18
Layered aquifer	0.231	$1.16\cdot10^{-5}$	10^{-4}	0.09	10^{-2}	4.18	$1.16\cdot10^{-8}$	10^{-4}	0.09	$2\cdot10^{-2}$	1.28	10^{-2}	4.18

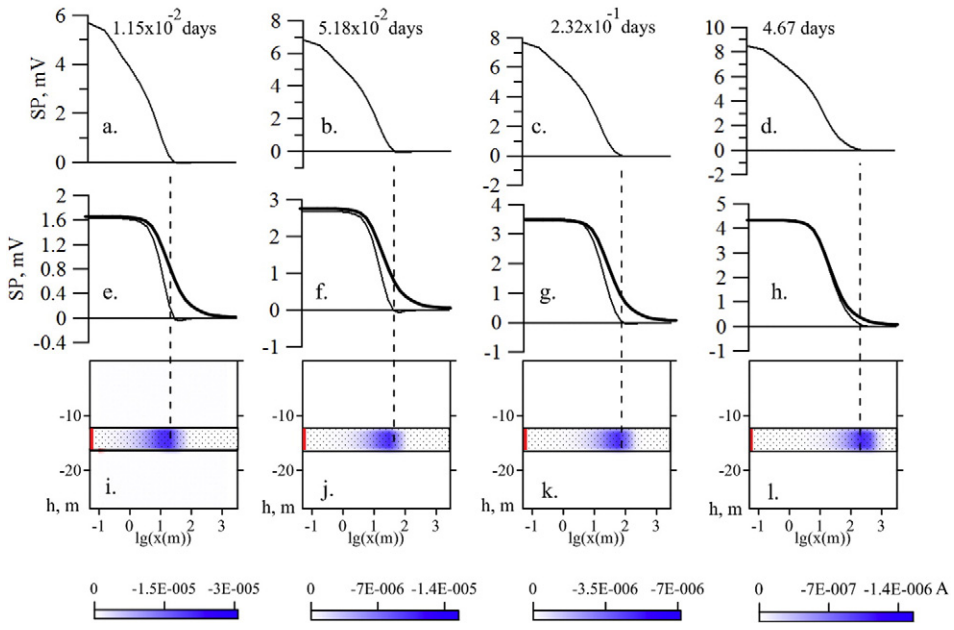

Fig. 1. Self-potential signals (a–h) and respective electrical sources (i–l), produced by a pumping test in an individual confined aquifer. Conductive casing of the pumping well: a–d; insulating casing of the pumping well: e–h; distribution of negative sources in Amperes: i–l. Note that a constant positive source ($+8.1.10^{-3}$ A) is located at the pumping well. For model parameters, see Table 1. The bold lines in panels e–h show the distributions of $SP \sim r^{-1}$, where r is the distances between the center of the pumping interval and the measurement point. The pumping well fully penetrates the aquifer on the left side of the model, and the aquifer is shown by dotted area. The reference electrode is 5 km away from the model centre.

(Press et al. 1992, p. 857). More details about this method applied to pumping test modeling can be found in, e.g., Titov et al., 2005.

1.4. Modeling results

First we modeled the SP signals in the case of a single confined aquifer (Fig. 1). The SP signals (Fig. 1a–h) are directly related to the electrical sources (Fig. 1i–l). The width of the SP anomaly is limited by the center of the negative source distribution in the aquifer. This results in a difference between the SP signals and the power law distribution $SP \sim r^{-1}$, and produces very small negative values of SP, which correspond to areas of transient flow regime. The intensity of the positive source located at the pumping well is three orders of magnitude greater than that of the negative sources distributed in the aquifer. We distinguished two cases: that of the conductive (metallic) casing of the pumping well, and that of the insulating (plastic) casing. The conductive casing attracts the electrical currents (e.g., Darnet et al., 2003), it serves as equipotential surface, which leads to a sharp SP distribution on the ground surface, in contrast to the case of the insulating casing. Fig. 2 illustrates this effect for the case of a single aquifer and homogenous distribution of the electrical conductivity.

Fig. 3 shows relationships between SP signals and the piezometric head variation at different times (counted from the beginning of the pumping test). In the conductive casing case, the SP signals are more closely related to the drawdowns than those in the insulating casing case (see, e.g., Titov et al. 2005).

For the layered aquifer (Fig. 4), the electrical source distribution is very different from the previous model. The intensity of the positive source located at the pumping well is comparable to that of the negative sources distributed within the layered aquifer. At an early time (Fig. 4 e),

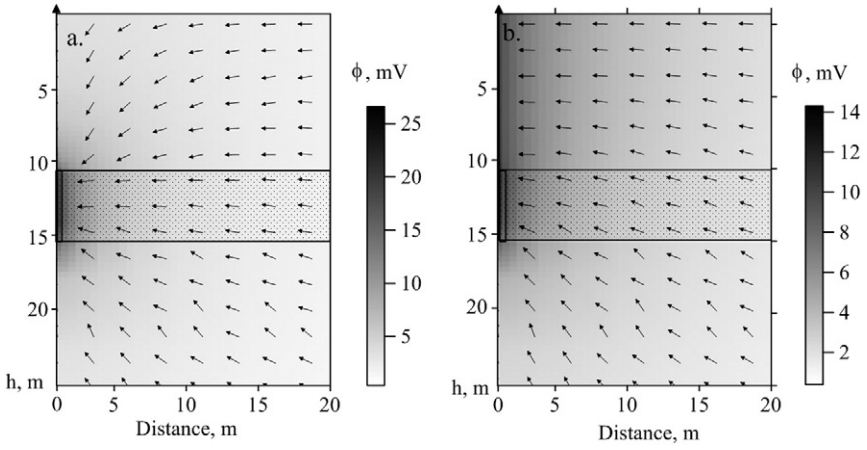

Fig. 2. Cross section of radial distribution of the electrical potential around the pumping well, which is located at distance $r = 0$. (The model is shown in Fig. 1). Only 20 m are shown for clarity. The reference electrode is 5 km away from the model centre. The aquifer is shown by dotted area, and the pumping interval is shown by the rectangle. The insulating and conductive casing cases are shown in panels (a) and (b), respectively. For the insulating casing, only the pumping interval is electrically conductive (with the same value of electrical conductivity as the host medium). Arrows show the distribution of the electrical field, which coincides with the electrical current density in a homogenous and isotropic medium.

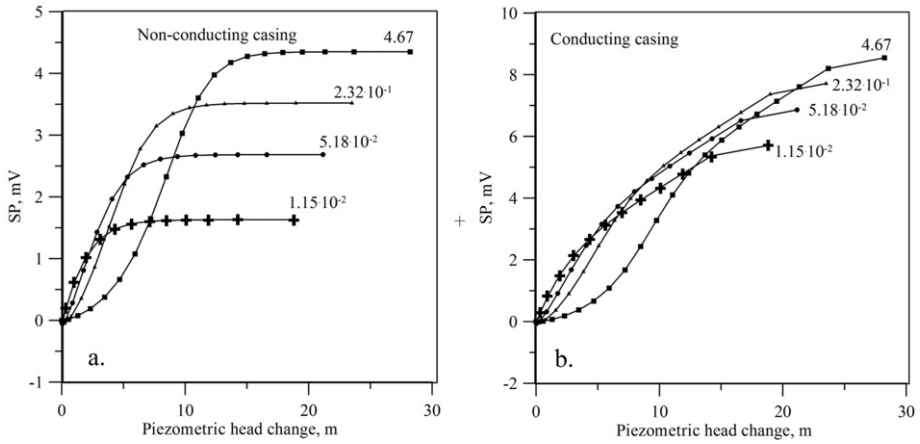

Fig. 3. SP signals vs. piezometric head change produced in the course of a pumping test in an individual confined aquifer. Different time moments are shown by numbers (in days); insulating (a) and conductive (b) casing of the pumping well. The intrinsic voltage coupling coefficient for the aquifer is -4.18 mV m^{-1}.

the negative sources are distributed at the top of the main aquifer and within the aquitard. These sources are responsible for the negative SP signals at the ground surface. The positive electrical signals are channeled to the ground surface in the case of the conductive casing only. As more time elapses, the center of the negative source distribution moves first toward the aquitard (Fig. 4f), and then toward the shallow aquifer (Fig. 4h). These negative sources indicate the downward groundwater flow from the shallow aquifer to the main aquifer. Note that, in the insulating casing case, the SP signals vary with time, but at any given moment they are almost constant within 10 m distance from the pumping well.

Fig. 5 shows relationships between the SP signals and the piezometric head variations at different times. In the insulating casing case, the SP signals are not sensitive to the piezometric head variations (Fig. 5a). In the conducting casing case, the relationships between the SP signals and the drawdowns contain quasi-linear parts (Fig. 5b). However, these relationships are specific for each time moment. The slopes of the relationships, which represent the apparent voltage coupling coefficient (see Rizzo et al., 2004), are similar (between 0.47 mV m^{-1} and 0.63 mV m^{-1}), but the constant term decreases with the time increase. This decrease of the constant term was explained by the near-surface negative sources produced by the downward flow from the shallow aquifer to the main aquifer (Fig. 4). The overall data fit shows a poor determination coefficient ($R^2 = 0.407$) with the slope of 0.252 mV m^{-1}, which is about twice lower than the average apparent voltage coupling coefficient for each of the data series.

2. Discussion

In the case of a single aquifer, SP signals monotonously increase with time. A simple data analysis can be based on a correlation between the SP signals and the piezometric head variations (see Fig. 3b). For a layered aquifer, the situation is totally different. The simple correlation-based analysis is not feasible because of a specific behavior of the downward groundwater flow (Fig. 5b).

Fig. 6 shows how the drawdown and SP signals vary with time at three selected points. Following Malama et al. (2009a, 2009b), in Fig. 6 we showed normalized parameters of the pumping test. We normalized the drawdown and the distance from the pumping well by the main aquifer thickness, b. We used the normalized time,

$$t_n = at/b^2, \tag{8}$$

where $a = K/S$ is the main aquifer diffusivity;
and the normalized SP,

$$SP_n = SP/SP_c, \tag{9}$$

$$\text{where } SP_c = \frac{Q}{4\pi bK}\frac{L}{\sigma}. \tag{10}$$

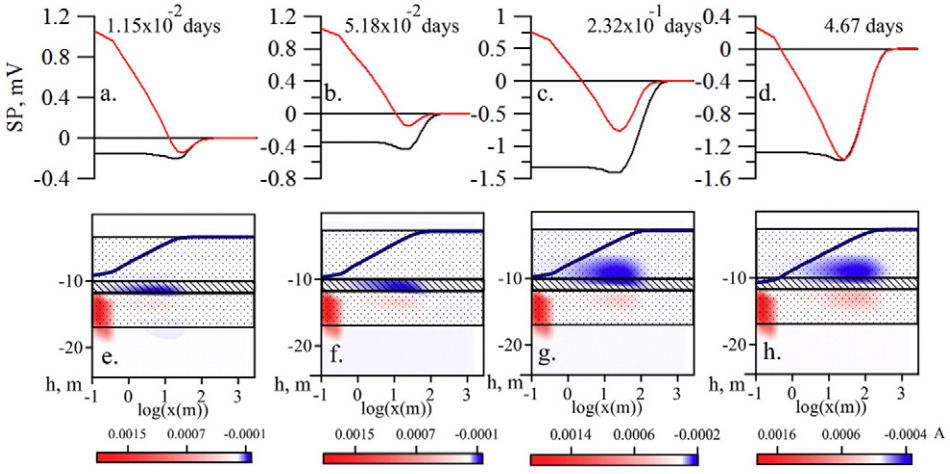

Fig. 4. Self-potential signals (a–d) and respective electrical sources in Amperes (e – h) produced by a pumping test in a layered aquifer. In SP distributions, black and red lines show the cases of insulating and conductive pumping well casings, respectively. For model parameters, see Table 1. The blue line shows the water head distribution in the main aquifer. The pumping well fully penetrates the main aquifer on the left side of the model. The aquifers and aquitard are shown by dotted and hatched layers, respectively. The reference electrode is 5 km away from the model centre.

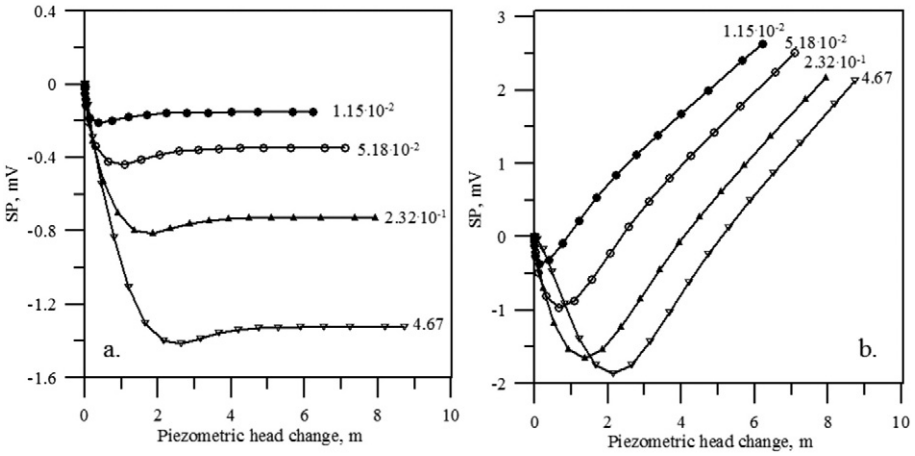

Fig. 5. SP signals vs. piezometric head change produced in the course of a pumping test in a layered aquifer. Different time moments are shown by numbers (in days); insulating (a) and conductive (b) casing of the pumping well. The intrinsic voltage coupling coefficient for the aquifer is 4.18 mV m^{-1}.

In the insulating casing case (Fig. 6c), the SP signals vs. time are almost independent of the distance from the pumping well, which is in agreement with the data shown in Fig. 4. However, in the conducting casing case, the SP signals behave quite differently. Fig. 6a,b shows coherent behavior of the drawdowns and the SP signals. Three phases of the pumping test can be specified. At early times (phase I), the main aquifer in conjunction with the aquitard act as a single aquifer, which produces logarithmic relationships "drawdown – time" (Fig. 6a) and "SP – time" (Fig. 6b). At significant distances from the pumping well, SP is not sensitive to the drawdown. In the intermediate time range (stage II), the downward flow from the shallow aquifer to the main aquifer starts and continuously intensifies. The SP signals decrease achieving negative values at 0.8 and 4.3 (the normalized distances). The negative SP values are consistent with those predicted by the Malama (2014) model. In his model, strong electrokinetic coupling in the vadose zone produces negative SP signals while the week coupling produces positive responses. This situation is similar to the models we studied. The case of strong coupling is close to the case of a layered aquifer, whereas the case of the weak coupling is close to the case of an individual aquifer, when the impact of the vadose zone can be neglected.

To illustrate the effect of the downward flow, we calculated separately the contribution of the vertical flow to the pumping rate, and defined the vertical-to-total flow rate, which was plotted as a function of the normalized time in Fig. 7. With the time increase, the vertical-to-total flow rate monotonously increases up to an asymptotic value of 50%, which was specific to our model. The vertical flow produces decreased slopes of drawdown (Fig. 6a), and results in a decrease of the SP signals (Fig. 6b,c). At late times (stage III), the main aquifer and the shallow aquifer begin to react to the pumping in conjunction. This leads to an increase of the drawdown slopes (Fig. 6a), and an increase of the SP signals (Fig. 6b, c). Therefore, the SP signals clearly denote three different stages in the pumping test.

Interestingly, the SP signals indicate the transitions from one stage to the next much earlier than the drawdowns. For the drawdown values, the first stage ends at 560 (the dimensionless time value), and for the SP signals it ends at the value of 1.87. Similarly, the second stage for the drawdown ends at about 10^5 (dimensionless time value), and for the SP signals it ends at the value of $1.4 \cdot 10^3$. This observation was explained by an inherent difference between the drawdowns and SP signals. The slope of drawdowns is controlled by the water sources in the main aquifer. The drawdown slope starts to decrease when about 30% of the water comes to the main aquifer from the shallow aquifer (Fig. 7). In contrast, SP signals are controlled by near-surface negative electrical sources produced directly by the downward flow (Fig. 4).

3. Conclusions

For the layered aquifer, the SP signals are very different from those associated with an individual confined aquifer. The "SP signals vs. drawdowns" dependencies display no universal correlation (within a pumping test framework) but show individual correlations specific for each time moment. Clearly, this is not a problem when the hydraulic conductivity distribution is obtained on the basis of optimization of both hydraulic head distribution and SP in steady state conditions (Soueid Ahmed et al., 2014). However, time diagrams of the drawdown and those of the SP signals are closely related. Both distributions show three stages of the pumping test: (I) when the main aquifer and the aquitard act in conjunction, as a single aquifer; (II) characterized by

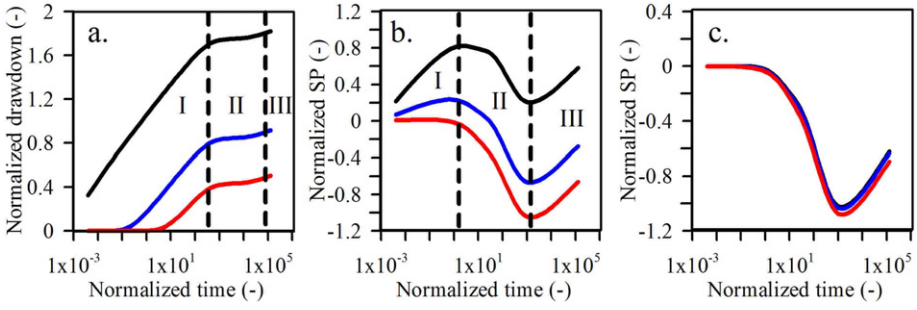

Fig. 6. Normalized drawdown (a) and normalized SP signals (b and c) for the cases of conductive (b) and insulating (c) pumping well casing. Graphs correspond to the normalized distances from the pumping well: 0 (black), 0.8 (blue) and 4.3 (red). Three phases of the pumping experiment are specified: I – "the early time", when the main aquifer and the aquitard act in conjunction, as a single aquifer; II – "the intermediate time", when the downward flow from the shallow aquifer determines the drawdowns and SP signals; and III — "the late time", when all three layers act in conjunction, as a single aquifer.

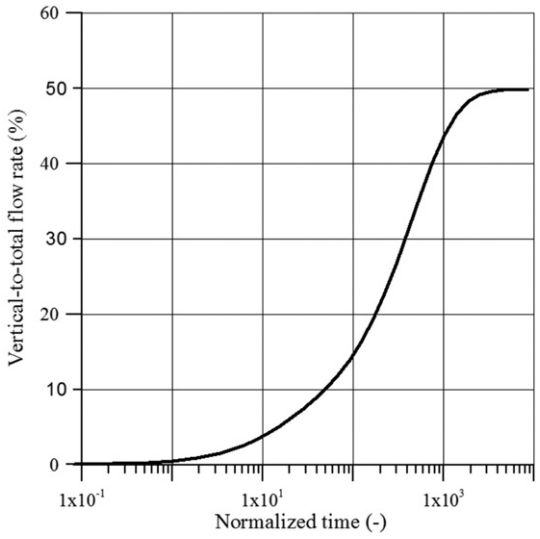

Fig. 7. Vertical-to-total flow rate vs. normalized time. The slopes of drawdowns (Fig. 6a) start to decrease at 560 (the dimensionless time value), when the vertical-to-total flow rate achieve the value of about 30%. In contrast, the SP signals (Fig. 6b) start to decrease in response to the vertical flow at 1.87 (the dimensionless time value), when the vertical-to-total flow rate achieve the value of about 1%.

the increased vertical-to-total flow ratio, which leads to the decreased slope of the drawdowns and decreased SP values; (III) when the main aquifer and the shallow aquifer start acting in conjunction, as a single aquifer. It is important to note that the SP signals show the beginnings of the second and third stages much earlier than the drawdowns, that is, show a "fast reaction". Therefore, our modeling results suggest that SP and piezometric data are complementary (in time scale) regarding determination of the aquifer parameters. (For the complementarity of SP signals and piezometric data in steady state conditions, see Soueid Ahmed et al. (2014)). Finally, the aforementioned "fast reaction" of SP signals to the pumping, in principle, allows reducing the duration of future pumping tests without losing valuable information.

Acknowledgments

This work was supported by St. Petersburg State University grant № 3.37.134.2014 -"Stimulated groundwater flow: experimental detecting and characterization using self-potential measurements".

References

Bolève, A., Revil, A., Janod, F., Mattiuzzo, J.L., Jardani, A., 2007. Forward Modeling and validation of a new formulation to compute self-potential signals associated with ground water flow. Hydrol. Earth Syst. Sci. 11, 1–11 (www.hydrol-earth-syst-sci.net/11/1/2007/).

Bolève, A., Revil, A., Janod, F., Mattiuzzo, J.L., Fry, J.-J., 2009. Preferential fluid flow pathways in embankment dams imaged by self-potential tomography. Near Surf. Geophys. 7, 447–462.

Bear, J., 1979. Hydraulics of Groundwater. McGraw Hill, New York.

Bogoslovsky, V.A., Ogilvy, A.A., 1973. Deformation of natural electric fields near drainage structures. Geophys. Prospect. 21, 716–723.

Chidichimo, F., De Biase, M., Rizzo, E., Masi, S., Straface, S., 2015. Hydrodynamic parameters estimation from self-potential data in a controlled full scale site. J. Hydrol. 522, 572–581. http://dx.doi.org/10.1016/j.jhydrol.2015.01.022.

Darnet, M., Marquis, G., Sailhac, P., 2003. Estimating aquifer hydraulic properties from the inversion of surface streaming potential (SP) anomalies. Geophys. Res. Lett. 30, 1679. http://dx.doi.org/10.1029/2003GL017631.

Gill, P.E., Murray, W., Saunders, M.A., 2005. SNOPT: an SQP algorithm for large-scale constrained optimization. SIAM Rev. 47 (1), 99–131. http://dx.doi.org/10.1137/S0036144504446096.

Gorelik, A.M., Nesterenko, I.P., 1956. Metod potentsialov elektrofil'tratsii pri opredelenii radiusa depressionnoi voronki v khode otkachki iz skvazhini. (Method of electro-filtration potential in the determination of radius of the depression cone during a pumping test from borehole, in Russian). Izv. Akad. Nauk. SSSR Ser. Geofiz. 11, 1361–1363.

Grunevald, U., 1971. Zur Anwendung Objektiver Methoden der Parameterschatzung auf Modellkonzepte der Abflubkoncentration. TU, Dresden.

Ishido, T., Mizutani, H., 1981. Experimental and theoretical basis of electrokinetic phenomena in rock–water systems and its applications to geophysics. J. Geophys. Res. 86, 1763–1775.

Jardani, A., Revil, A., Barrash, W., Crespy, A., Rizzo, E., Straface, S., Cardiff, M., Malama, B., Miller, C., Johnson, T., 2009. Reconstruction of the water table from self-potential data: a Bayesian approach. Ground Water 47, 213–227.

Malama, B., Revil, A., Kuhlman, K.L., 2009a. A semi-analytical solution for transient streaming potentials associated with confined aquifer pumping tests. Geophys. J. Int. 176, 1007–1016. http://dx.doi.org/10.1111/j.1365-246X.2008.04014.x.

Malama, B., Kuhlman, K.L., Revil, A., 2009b. Theory of transient streaming potentials associated with axial-symmetric flow in unconfined aquifers. Geophys. J. Int. 179, 990–1003. http://dx.doi.org/10.1111/j.1365-246X.2009.04336.x.

Malama, B., 2014. Theory of transient streaming potentials in coupled unconfined aquifer-unsaturated zone flow to a well. Water Resour. Res. 50, 2921–2945. http://dx.doi.org/10.1002/ 2013WR014909.

McDonald, M.C., Harbaugh, A.W., 1988. *MODFLOW*, a modular threedimensional finite difference ground-water flow model: U.S. Geological Survey. Open-file report 83–875 (Chapter A1).

Murashko, A.M., Khasenevich, B.K., Firsiuk, P.I., 1981. Vremennie recomendatsii po premeneniu geofisicheskikh metodov pri iziskaniyakh dlia meliorativnogo stroitel'stva v usloviakh BSSR. (Recommendations for use of geophysical methods for investigations for amending construction in BSSR, in Russian), Belnii MVH, Minsk.

Ozaki, Y., Mikada, H., Goto, T., Takekawa, J., 2014. The 3D self-potential inversion for the estimation of hydraulic parameters. SEG 2014 Annual Meeting, SEG, Expanded Abstracts, pp. 4539–4543 http://dx.doi.org/10.1190/segam2014-1104.1.

Press, W.H., Teucolsky, S.A., William, T., Vetterling, W.T., Flannery, B.P., 1992. Numerical Recipes. The Art of Scientific Computing. third ed. Cambridge University Press, Cambridge.

Revil, A., Leroy, P., 2004. Constitutive equations for ionic transport in porous shales. J. Geophys. Res. 109, B03208. http://dx.doi.org/10.1029/2003JB002755.

Revil, A., Mahardika, H., 2013. Coupled hydromechanical and electromagnetic disturbances in unsaturated porous materials. Water Resour. Res. 49. http://dx.doi.org/10.1002/wrcr.20092.

Rizzo, E., Suski, B., Revil, A., Straface, S., Troisi, S., 2004. Self-potential signals associated with pumping tests experiments. J. Geophys. Res. 109, B10203. http://dx.doi.org/10.1029/2004JB003049.

Semenov, A.S., 1981. Elektrorazvedka Metodom Estestvennogo Elektricheskogo Polia. (Electrical Prospecting with the Natural Electric Field Method, in Russian). second ed. Nedra, Leningrad.

Soueid Ahmed, A., Jardani, A., Revil, A., Dupont, J.P., 2014. Hydraulic conductivity field characterization from the joint inversion of hydraulic heads and self-potential data. Water Resour. Res. 50 (4), 3502–3522. http://dx.doi.org/10.1002/2013WR014645 (1914).

Sill, W.R., 1983. Self-potential modeling from primary flows. Geophysics 48, 76–86.

Straface, S., Rizzo, E., Gianpaolo, V., Chidichimo, F., 2011. Estimation of hydraulic conductivity in a large scale laboratory model by means of the self-potential method. Int. Water Technol. J. 1, 1–15.

Suski, B., Revil, A., Titov, K., Konosavsky, P., Voltz, M., Dagès, C., Huttel, O., 2006. Monitoring of an infiltration experiment using the self-potential method. Water Resour. Res. 42, W08418. http://dx.doi.org/10.1029/2005WR004840.

Titov, K., Revil, A., Konosavsky, P., Straface, S., Troisi, S., 2005. Numerical modelling of self-potential signals associated with a pumping test experiment. Geophys. J. Int. 162, 641–650. http://dx.doi.org/10.1111/j.1365-246X.2005.02676.x.

Vasconcelos, S.S., Mendonça, C.A., Silva, N., 2014. Self-potential signals from pumping tests in laboratory experiments. Geophysics 79, EN125–EN133. http://dx.doi.org/10.1190/GEO2013-0444.1.